IEEE Transactions on Nuclear Science, Vol. NS-28, No. 3, June 1981

THREE-DIMENSIONAL SPACE CHARGE CALCULATION METHOD*

W. P. Lysenko and E. A. Wadlinger
Los Alamos National Laboratory, Los Alamos, NM 87545

Summary

We present a method for calculating space-charge forces suitable for use in a particle tracing code. We solve Poisson's equation in three dimensions with boundary conditions specified on an arbitrary surface by using a weighted residual method. Using a discrete particle distribution as our source input, examples are shown of off-axis, bunched beams of noncircular crosssection in radio-frequency quadrupole (RFQ) and drift-tube linac geometries.

Introduction

To determine the space-charge forces in an accelerator particle tracing simulation we would like to solve the Poisson equation,

$$\nabla^2\phi = -\rho \quad , \tag{1}$$

in a region V, with a homogeneous boundary condition on the surface S bounding the region,

$$\phi(\vec{x}) = 0 \text{ on } S \quad . \tag{2}$$

Inhomogeneous boundary conditions are not required because we assume that we know the external electrostatic fields. We want to calculate the electrostatic fields generated by the charged particle bunch in the presence of a perfectly conducting boundary. Both the source and the boundary will be assumed to be periodic in the z-direction.

Method

Expand the potential in a finite set of n known functions ϕ_i

$$\phi = a_i\phi_i \quad . \tag{3}$$

(Repeated indices are summed over.) The coefficients a_i are to be determined. The functions ϕ_i must form as complete a set as possible. (This will require n to be large.) Now define a residual R that has a volume and a surface part

$$R_V = a_i \nabla^2 \phi_i + \rho \quad ,$$

$$R_S = a_i\phi_i \quad . \tag{4}$$

These residuals are zero when Eqs. (1) and (2) are satisfied. The method of weighted residuals[1] sets the weighted average of the residual to zero, resulting in n conditions on the a_i.

$$0 = \int_V dV(a_i\nabla^2\phi_i+\rho)w_j + w\int_S dS a_i\phi_i w_j \quad , \; j=i,\ldots,n \tag{5}$$

The $w_j(\vec{x})$ are the weight functions and w is a weight that can be adjusted according to the desired relative importance of the volume and surface terms. Equation (5) may be written in matrix form as

$$M_{ij}\, a_j = S_i \quad , \tag{6}$$

where the matrix M_{ij} and the source vector S_i are given by

$$M_{ij} = \int_V dV\ \nabla^2\phi_i w_j + w\int_S dS\phi_i w_j \quad ,$$

$$S_i = -\int_V dV\rho w_i \quad . \tag{7}$$

The matrix M_{ij} depends only on the geometry and can be computed numerically, if necessary, for complex geometries. The source term depends on the charge distribution and must be computed at every time step in the particle tracing simulation. For discrete particle distributions, the source vector is simply a sum over particles of the quantity $-w_i(\vec{x}_p)$ where $\vec{x}_p$ is the particle coordinate. Because we must invert the matrix to solve for the coefficients a_i in Eq. (6), it is important to choose expansion functions that are linearly independent.

We will consider two types of weighted residual methods. The first is the least-squares method in which $w_i = \partial R/\partial a_i$. With this choice, the condition of Eq. (5) minimizes the quantity $\int dV R_V^2 + w\int dS R_S^2$. The second type of weighted-residual method is the Galerkin method in which $w_j = \phi_j$. With this choice the condition of Eq. (5) becomes $0 = \int dV R_V\phi_i + w\int dS R_S\phi_i$. This procedure finds the correct solution by requiring the residual, which is zero for the exact solution, to be orthogonal to a (nearly) complete set of functions, the expansion functions themselves. The Galerkin method is preferable for our problem for two reasons. First, it is easier to calculate the matrix and source term because the weight functions do not involve Laplacians of the expansion functions. The second reason is related to the fact that because the finite set of expansion functions is not complete, both methods give only approximate solutions. As mentioned above, the least-squares method minimizes the error in the square of the residual. This means that the error in the fitted charge density, $-a_i\nabla^2\phi_i$ is minimized. But we are interested in the field generated by the charge; that is, we would like to minimize the error in $-a_i\nabla\phi_i$. We can show that the Galerkin condition minimizes $\int dV(a_i\nabla\phi_i - \nabla\phi)^2$, provided that the expansion functions vanish on the surface S. The condition that the ϕ_i vanish on the boundary is easy to satisfy for our examples. Furthermore, because the ϕ_i vanish exactly on the surface, there is no danger from the dynamical effect of beam-wall interactions.

Thus we consider the following Galerkin problem

$$M_{ij} = M_{ji} = \int_V dV\ \nabla^2\phi_i\ \phi_j,$$

$$S_i = \int_V dV\rho\phi_i \quad . \tag{8}$$

*Work performed under the auspices of the U. S. Department of Energy.

0018-9499/81/0600-2509$00.75©1981 IEEE

For the case of a cylindrical boundary condition we use the following expansion functions (in polar coordinates)

$$\phi_i(r,\theta,z) = \left[1-\left(\frac{r}{r_o}\right)^2\right]\left(\frac{r}{r_o}\right)^{n_i} \begin{Bmatrix}\cos m_i\theta \\ \sin m_i\theta\end{Bmatrix} \begin{Bmatrix}\cos 2\pi k_i z/L \\ \sin 2\pi k_i z/L\end{Bmatrix} \quad (9)$$

where L is the period length and r_o is the radius of the conducting cylinder. For the RFQ structure, we multiply the above by the RFQ factor

$$F = \left[(1-A)\left(\frac{r}{a}\right)^2 \cos 2\theta + A\cos 2\pi z/L\right]^2 - 1 \quad (10)$$

which causes the ϕ_i to vanish on the RFQ vanes. We use the notation of Ref. 2 in which a is the minimum vane radius and A is the acceleration efficiency parameter (A = 0 for no vane modulation).

If the expansion functions are ordered so that all functions with a given z-harmonic are grouped together, the matrix of Eq. (8) becomes block-diagonal for the case of the cylinder. The number of blocks is $2k_{max}+1$ where k_{max} is the highest z-harmonic. This problem is equivalent to $2k_{max}+1$ transverse problems in which only small (95 x 95 in our examples) matrices have to be inverted. For the RFQ case on the region $r \leq r_o$, the matrix has five block diagonals. To solve this system we use the following iterative procedure. Decompose the matrix into two parts

$$M = M_D + M_R \quad (11)$$

where M_D is the block-diagonal part and M_R is the remainder of the matrix. The solution (expansion coefficients) can be obtained by iterating using the following relation

$$a_{I+1} = M_D^{-1}(S - M_R a_I) \quad . \quad (12)$$

The subscripts on the a's are the iteration numbers. Only the easy-to-invert matrix M_D has to be inverted in this procedure.

Testing

We used the following charge-density distribution

$$\rho = \begin{cases} 1 - \bar{r}^2 + \bar{r}^4/4 & , \bar{r} \leq 2^{1/2} \\ 0 & , \bar{r} > 2^{1/2} \end{cases} \quad (13)$$

where

$$\bar{r}^2 = \left(\frac{x-x_c}{x_o}\right)^2 + \left(\frac{y-y_c}{y_o}\right)^2 + \left(\frac{z-z_c}{z_o}\right)^2 \quad (14)$$

in which the bunch center is at (x_c,y_c,z_c) and the bunch half-lengths are $2^{1/2}x_o$, $2^{1/2}y_o$, and $2^{1/2}z_o$. We transform this charge distribution to a discrete particle distribution, which would be found in a particle tracing code, as follows. Choose a particle coordinate $\vec{x}$ within V at random and evaluate $\rho(\vec{x})$, which ranges from zero to one in our example. Now choose another (a fourth) random number between zero and one. If this new random number is less than $\rho(\vec{x})$ we keep $\vec{x}$ as the position of a particle in our discrete distribution. Otherwise, this particle is rejected and we start again by choosing a new particle position. This procedure is continued until the desired number of particles (10 000 in our examples) is reached. The result is a discrete distribution that in the large particle-number limit has the charge distribution ρ.

Using this source distribution we can form the source vector and solve Eq. (6) to get the coefficients a_i. Because we can compute the gradients of the known expansion functions ϕ_i, the desired approximation for the electric field is

$$E_a = -a_i \nabla\phi_i \quad . \quad (15)$$

But the exact field is unknown, so we have no means of determining the accuracy of this approximation. We can, however, compute the approximate charge density

$$\rho_a = -a_i \nabla^2\phi_i \quad , \quad (16)$$

which can be compared with the input density ρ of Eq. (13). We can form a discrete particle distribution from ρ_a in the same manner that we did from the input density ρ. Then, scatter plots of ρ and ρ_a can be directly compared. Because the approximation is not exact, there are regions of negative charge density so our scatter-plot output consists of two plots, one for each sign of charge.

Examples

We did two examples, one with a circular cylindrical boundary condition, which would be applicable to a drift-tube linac, and one with an RFQ boundary condition. Except for the RFQ factor F, the same expansion functions were used for both cases. The maximum power of r was n = 8, the highest θ-harmonic was m = 8, and the highest z-harmonic was k = 6. For the lower values of n ($n \leq 3$), only those m-values were used that made these terms smooth (powers of x and y). Higher n-value terms were permitted to have discontinuities in higher derivatives at the origin. The number of expansion functions was 1235 (95 transverse x 13 z-terms).

We used the same source for both examples. The beam was centered at x = 0.37, y = 0.26, z = 0.50 (r = 0.45, θ = 35°). The half sizes were $2^{1/2}x_o = 0.71$, $2^{1/2}y_o = 0.42$, and $2^{1/2}z_o = 0.49$.

Cylinder

The radius of the cylindrical region was $r_o = 1.3$ and its length (period) was L = 2. Figure 1 shows scatter plots with outlines of the region boundary. From left to right, we see the projections onto the x-y, z-x, and z-y planes. The first row shows 2000 of the 10 000 particles used to represent the input distribution. The second row shows the equivalent plots for a 2000-particle representation of the fitted charge distribution Eq. (16). Only positive charges are shown here. The third row shows the scatter plots for the negative charge distribution arising from the errors in the approximate solution. There are 176 negative particles that correspond to the 2000 positive particles. These scatter plots are very sensitive indicators of errors in the fitted charge distribution. (Because the particle density in the region of the bunch is so high, the eye cannot distinguish how many particles are in the black region, while the other particles in the volume,

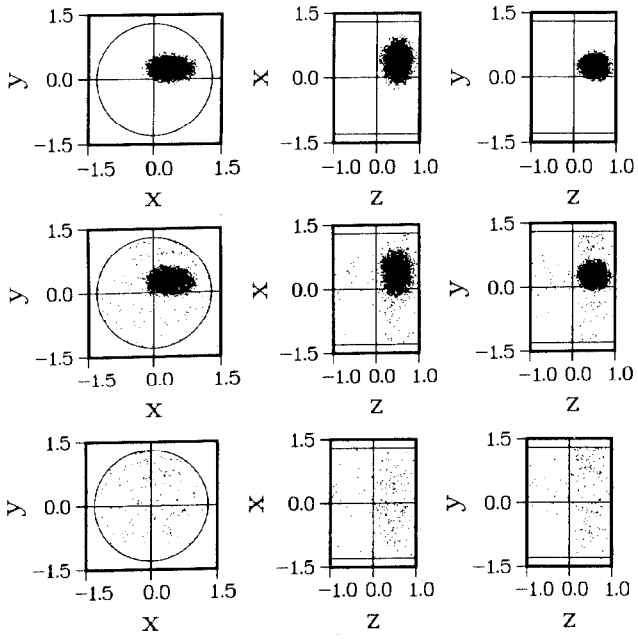

Fig. 1. Scatter plots for the cylindrical boundary case. The first row shows 2000 of the 10 000 particles used to represent the input distribution. The second row shows a 2000-particle representation of the positive part of the fitted charge distribution. The third row shows the scatter plots for the negative charge distribution arising from the errors in the approximate solution. There are 176 negative particles.

which correspond to an error charge, become relatively more apparent. Also, these error particles are projected from the whole volume of the region, which is much larger than the bunch volume, thus enhancing the visibility of the charge errors.)

Figure 2 shows the charge-density profiles at the bunch center. For example, the x-profile is $\rho_a(x,y_c,z_c)$ plotted as a function of x. Both the exact and fitted profiles are plotted. In this case, the fit is so good that the curves are almost indistinguishable.

Figure 3 shows equipotential contours (fitted potential) for various sections along with the boundary outline. The contours represent 0.9, 0.8, 0.7,

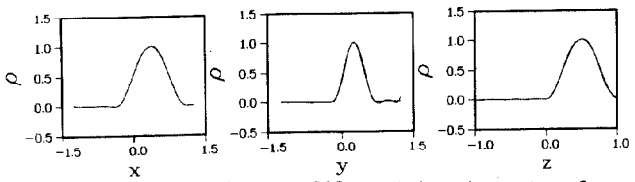

Fig. 2. Charge density profiles at bunch center for the cylindrcial boundary case. For example, the first plot shows $\rho(x,y_c,z_c)$ plotted as a function of x where the bunch center is at (x_c,y_c,z_c). Both the input charge distribution and the approximate solution are plotted. The curves are almost indistinguishable in this case.

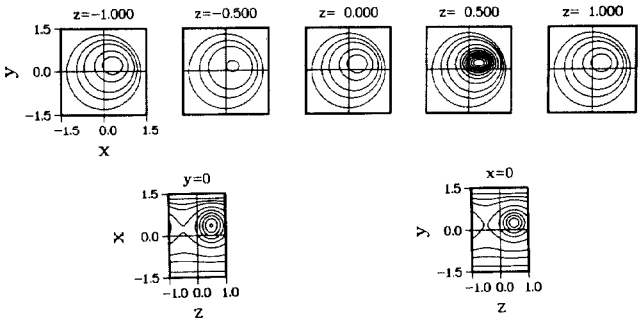

Fig. 3. Equipotential contours various sections for the cylindrical boundary case. The contours represent 0.9, 0.8, 0.7, 0.6, 0.5, 0.4, 0.3, 0.2, 0.1, and 0.05 of the maximum value. Only the x-y section at z = 0.5 has all ten contours because only this section contains the bunch center. Others have lower potentials.

0.6, 0.5, 0.4, 0.3, 0.2, 0.1, and 0.05 of the maximum value. (Only the x-y section at z = 0.5 has all ten contours because only this section contains the bunch center. Others have lower potentials.) The periodicity in z of the solution is evident from this figure.

RFQ

For the RFQ example, we used a minimum radius of a = 1.0 and an acceleration efficiency of A = 0.18 (corresponding to a modulation factor of m = 1.2). Only the first iteration of Eq. (12) (block-diagonal part only) was used. The iteration procedure converged, but did not improve the results. The integrals in the maxtrix elements were done numerically and numerical errors may have caused this effect. Figure 4

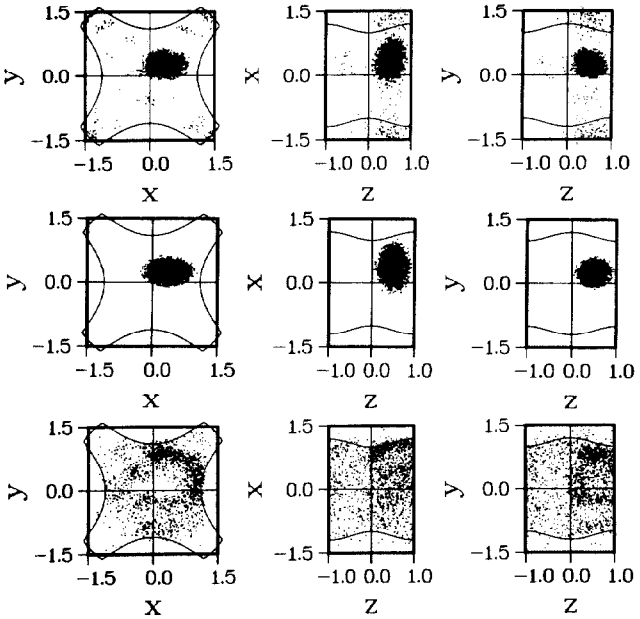

Fig. 4. Scatter plots for the radio-frequency quadrupole (RFQ) case. The first row shows 2000 of the 10 000 particles used to represent the input distribution. The second row shows a 2000-particle representation of the positive part of the fitted charge distribution. The third row shows scatter plots for the negative charge distribution arising from the errors in the approximate solution. There are 1543 negative particles.

shows the projections of the particles on the x-y, z-x, and y-z planes. The cross sections of the RFQ region in these planes are shown also. Because the RFQ region is not constant along the projection direction, some of the particles lie outside the RFQ outline on the projection surface. As in the case of the cylinder, the first row shows a 2000-particle sample of the input distribution and the second row shows a 2000-particle representation of the positive part of the fitted charge distribution. The third row shows the scatter plots for the negative part of the fitted charge distribution. There are 1543 negative particles.

Figure 5 shows the input and fitted charge-density profiles for the RFQ case. Figure 6 shows the equipotential plots at various sections for the RFQ case.

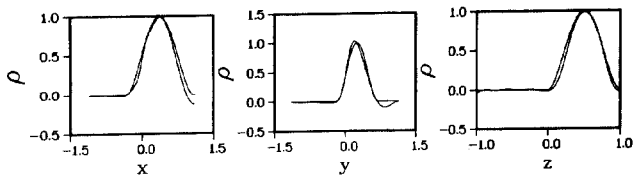

Fig. 5. Charge density profiles at bunch center for the RFQ case. For example, the first plot shows $\rho(x, y_c, z_c)$ plotted as a function of x where the bunch center is at (x_c, y_c, z_c). Both the input charge distribution and the approximate solution are plotted.

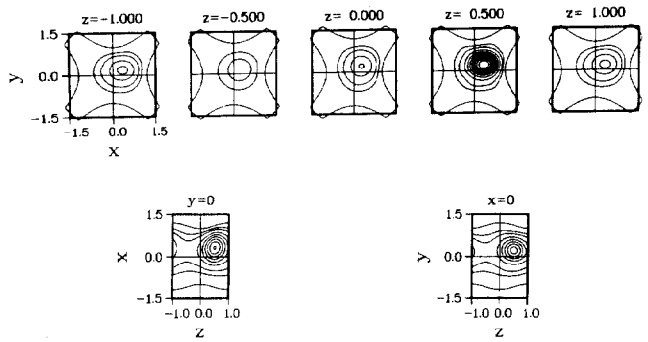

Fig. 6. Equipotential contours at various sections for the RFQ case. The contours represent 0.9, 0.8, 0.7, 0.6, 0.5, 0.4, 0.3, 0.2, 0.1, and 0.05 of the maximum value. Only the x-y section at z = 0.5 has all ten contours because only this section contains the bunch center. Others have lower potentials.

Discussion

Particle tracing codes for accelerator simulation require three-dimensional space-charge calculations in various geometries. The examples here show that the proposed method may be practical for such calculations. The cylindrical boundary case is especially accurate. Calculation of the maxtrix requires 1.3 s on a Cray-1 computer. Evaluation of the expansion coefficients takes about 12.5 s for 10 000 particles (mostly for evaluating the source vector, which has not been computationally optimized yet.) The RFQ case will require further development. It is evident that present results are not as accurate as for the cylindrical case, and the matrix computation requires much more computer time (~ 1/2 hours), because it is done numerically. We can, however, calculate the RFQ maxtrix analytically and will do so in the future. Besides drastically reducing computer-time usage, this should also improve the accuracy of the fit. (Fewer integration points in the numerical integration noticeably worsens the fit.) With this improvement, the off-block-diagonal maxtrix elements in the iterative procedure may further improve the fit. In all cases tried the statistical error in the coefficients, that is due to the finite number of particles in the distribution, is small compared to the fitting errors.

Acknowledgments

We thank B. Godfrey for suggesting that non-orthogonal expansions be used to calculate space charge, R. Cooper for his contributions in an unpublished report, and P. Channell for his contributions arising from numerous discussions.

References

1. B. A. Finlayson, The Method of Weighted Residuals and Variational Principles, (Academic Press, New York, 1972).

2. K. R. Crandall, R. H. Stokes, and T. P. Wangler, "RF Quadrupole Beam Dynamics Design Studies," Proc. 1979 Linear Accelerator Conf., Brookhaven National Laboratory report BNL 51134.